Unconventional density dependence of the stochastic dynamics in an organic liquid

A. Maira-Vidal,[1] M. A. González,[2] M. Jimenez-Ruiz,[2] F. J. Bermejo,[3,1] D. L. Price,[4,5] E. Enciso,[6] M. L. Saboungi,[7,5] R. Fernández-Perea,[1] and C. Cabrillo[1]

[1]*Instituto de Estructura de la Materia, C.S.I.C., Serrano 123, E-28006 Madrid, Spain*

[2]*Institut Laue Langevin, BP 156x, F-38042 Grenoble Cedex 9, France*

[3]*Department of Electricity and Electronics, University of the Basque Country, P.O. Box 644 Bilbao 48080, Spain*

[4]*Centre de Recherches sur les Matériaux à Haute Temperature, C.N.R.S. Orléans, France*

[5]*Argonne National Laboratory, Argonne, Illinois 60439, USA*

[6]*Departamento de Quimica-Fisica I, Facultad de Ciencias Quimicas, Universidad Complutense de Madrid, E-28080 Madrid, Spain*

[7]*Centre de Recherches sur le Matière Divisée, Universitè d'Orlèans–CNRS, 45071 Orléans Cedex 2, France*

(Received 11 February 2004; revised manuscript received 21 May 2004; published 9 August 2004)

The density dependence of the diffusive rotational and center-of-mass dynamics of 2-methyl-pyridine is investigated by means of the concurrent use of quasielastic neutron scattering and molecular dynamics simulations. The dependence of both translation and rotational diffusion coefficients shows a distinctive change of slope with increasing density taking place about $\rho = 0.975$ g/cm^3. Such a change in the dynamics can be related to observations made in other liquids composed of oblate-spheroidal particles.

DOI: 10.1103/PhysRevE.70.021501 PACS number(s): 61.12.−q, 61.20.Ja

I. INTRODUCTION

The rich variety of phase behaviors shown by mixtures of methyl-substituted pyridines (MP) and heavy or light water has attracted interest since the first characterization of their anomalous phase diagrams [1]. Similar phenomena have been known since the pioneering work by Hudson [2] on nicotine-water mixtures. The interest behind such studies stems from the opportunity offered by binary mixtures of MP and heavy water to deepen into knowledge of mechanisms leading to physical reentrance. In other words, these binary mixtures show a complex phase behavior as manifested by a closed-loop phase diagram as that shown in Fig. 1.

More into specifics, the system depicted in Fig. 1 becomes fully miscible outside the loop but separates into two macroscopically distinguishable phases when the low or high critical solution temperatures T_L and T_U are approached from below or above, respectively. Such a phenomenon is known as reentrance, since it characterizes a physical system that, driven by a monotonous change of a thermodynamic field (composition, density, temperature, etc.), reenters a phase similar to the initial state. Rather than confined to binary fluid mixtures it is common to a wide variety of physical systems comprising ferroelectrics, liquid crystals, antiferromagnets, or spin glasses [3].

While the presence of a miscibility line at T_U is easy to understand on energetic grounds, the fact that the mixture becomes miscible below T_L remains to be understood on quantitative grounds. The microscopic origin for this low-temperature mixing phenomenon is most of the time interpreted on the basis of a conjecture brought forward by Hirschfelder a long time ago [3]. It attributes remixing below T_L to the presence of strong directional bonding interactions between the two unlike species. On the other hand, very recent reports on a novel phase behavior where a tenuous solidlike structure appears at the liquid/liquid interface [4] make microscopic investigations of the forces driving such systems timely and well overdue.

The advantage of studying mixtures of MP and heavy water as physical realizations of reentrant systems over other solid-state materials stems from the ease of controlling the width of the inmiscibility loop. In fact, it is known that the loop size shows a extreme sensitivity to the isotopic composition of the hydrogen element (light or heavy water), the presence of salts [5], or the application of pressure [3]. This opens up a route to study critical phenomena of a special kind such as those leading to double critical points (DCP's), where renormalization-group theory predicts an exact dou-

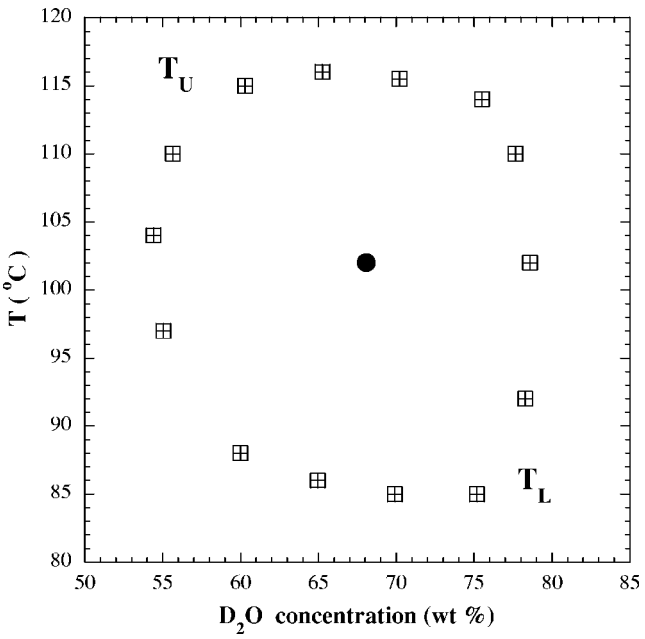

FIG. 1. Schematic phase diagram for a mixture of 2MP and heavy water. Data for ≈1 bar taken from Garland *et al.* [8] are shown by open lozenges. The solid dot depicts the estimated location of the double critical point that is ≈200 bar, 101 °C.

bling of the critical exponents corresponding to the Ising universality class [3,6].

Recently [7], we have undertaken a study of the microscopic processes leading to phase separation in MP/heavy-water mixtures by means of the concurrent use of NMR, small-angle, quasielastic neutron scattering (QENS), and molecular simulations. As a main result, the effects brought forward by the divergent behavior of the macroscopic shear viscosity on the microscopic transport coefficients were exemplified by the behavior exhibited by the translational diffusion coefficient measured using QENS as the temperature approached T_L from below.

As a further step, we have undertaken a study on the microscopic dynamics of a mixture of 2-methyl pyridine (2MP) and heavy water as one approaches a DCP by means of the application of moderate pressures [8]. As a preliminary study, we have carried out measurements on the density dependence of the rotational and translational diffusion coefficients of 2MP. These were needed as background data and were unavailable from previous experiments [8]. The outcome of such a study turned out to be surprising and of interest *per se* since the results portray a nonmonotonous behavior of the latter with increasing density for a range of pressures up to 1200 bars. We have then tried to understand the origin of such behaviors by means of molecular dynamics simulations carried out for a simple but realistic enough molecular model to represent the interactions between 2MP molecules. As described below, the results found from experiment and computer simulations depict a rather more complicated picture than initially thought of, since directional bonding interactions are present in both components making the reentrant mixture.

II. EXPERIMENTAL DETAILS

Fully hydrogenated 2-methyl-pyridine was used without further processing. The quasielastic neutron scattering measurements were carried out using the IN6 time-of-flight spectrometer of the Institute Laue Langevin (Grenoble). The incident wavelength used was 5.9 Å, giving an elastic energy resolution [full width at half maximum (FWHM)] of 50 μeV ($\approx$76 ns^{-1}) and covering a usable constant-Q range between 0.4 and 1.4 Å^{-1}. The sample was contained into a pressure cell where pressure was directly applied by a piston to a system full of liquid sample. The range of measured pressures was from 1 to 1200 bars. All the measurements were done at the same temperature of 40 °C with an accuracy of 0.5 °C. The data were corrected following the normal procedure (background subtraction, self-absorption corrections, normalization) and grouped and transformed into constant-Q spectra using ILL standard programs [9].

III. DATA ANALYSIS AND RESULTS

The coherent and incoherent scattering cross sections per molecule are 56.7 and 562.3 barns, respectively. This implies that scattering is mostly (91%) incoherent. Moreover, the available Q range comprises a region well below the maxima shown by the lowest momentum-transfer peak appearing in the static structure factor arising from the small coherent cross section. On such grounds the analysis of the double-differential scattering cross section is carried out within the incoherent scattering approximation, this meaning that all scattering is attributed to molecular protons.

Two contributions to the spectra were considered: translation and rotation of the molecules about their center of mass. The translational contribution is well accounted for by a Lorentzian line having a linewidth that approaches the $D_{\mathrm{T}}Q^2$ prescription given by the Fick diffusion law at low wave vectors, where D_{T} stands for the translational self-diffusion coefficient. Molecular rotations were described by the Sears expansion for hindered rotations over a sphere [10]. As customarily followed in work concerning high-temperature liquids the assumption of the statistical independence of translation and rotation is taken so that the translation linewidth gives rise to the Q-dependent spectral component and those corresponding to molecular reorientations give rise to higher-order components in the above-mentioned partial-wave expansion whose Q dependence is only limited to their amplitudes.

The rotation of the methyl group is too fast to be considered here as can be seen from values for the methyl rotational diffusion coefficients reported for analogous compounds such as toluene and some of its derivatives [11] (i.e., $D_{\mathrm{r}} > 1$ ps^{-1}). Further indication of the scant contribution of methyl-group rotations to our frequency window is given by the fact that it was not necessary to include it to obtain a good fit of all the spectra. The resulting expression employed to fit all spectra is given by

$$S_{obs}(Q,\omega) = \left(\frac{A_1}{\pi} \frac{\Gamma_{trans}}{(\omega-\omega_0)^2 + \Gamma_{trans}^2} + \frac{A_2}{\pi} \sum_{l=1}^{5} (2l+1) j_l^2(QR_H) \frac{\Gamma_{rot}^{(l)}}{(\omega-\omega_0)^2 + (\Gamma_{rot}^{(l)})^2} \right) \otimes R(Q,\omega) + \text{background}, \quad (1)$$

where the symbol $\otimes$ stands for convolution with the instrumental resolution, $R_H \simeq 2.47$ Å is the average distance of the hydrogen atoms to the molecular center of mass, and ω_0 is the (instrumental) offset. The molecular geometry thus makes terms with $l > 5$ negligible as $j_{l+1}/j_l \ll 1$ for $Q \leqslant 1.4$ Å^{-1}.

All spectra for a given pressure were fitted sequentially using a common parameter set. The estimates for the linewidth of the translational diffusion components were given by $\Gamma_{trans} = D_{\mathrm{T}}Q^2$, and the widths of the rotational lines are $\Gamma_{rot} = D_{\mathrm{T}}Q^2 + l(l+1)D_{\mathrm{r}}$, D_{r} being the isotropic rotational diffusion coefficient. Notice that both diffusion coefficients are taken as common parameters for every set of Q values. The arguments of the spherical Bessel functions j_l are set from the molecular geometry and "background" is a linear background. Good fits, shown in Fig. 2, were obtained when the relative weights of the translation and rotational components given by $A_{1,2}$ were allowed to deviate somewhat from unity, which is the value set for isotropic rotational and translational long-range diffusion.

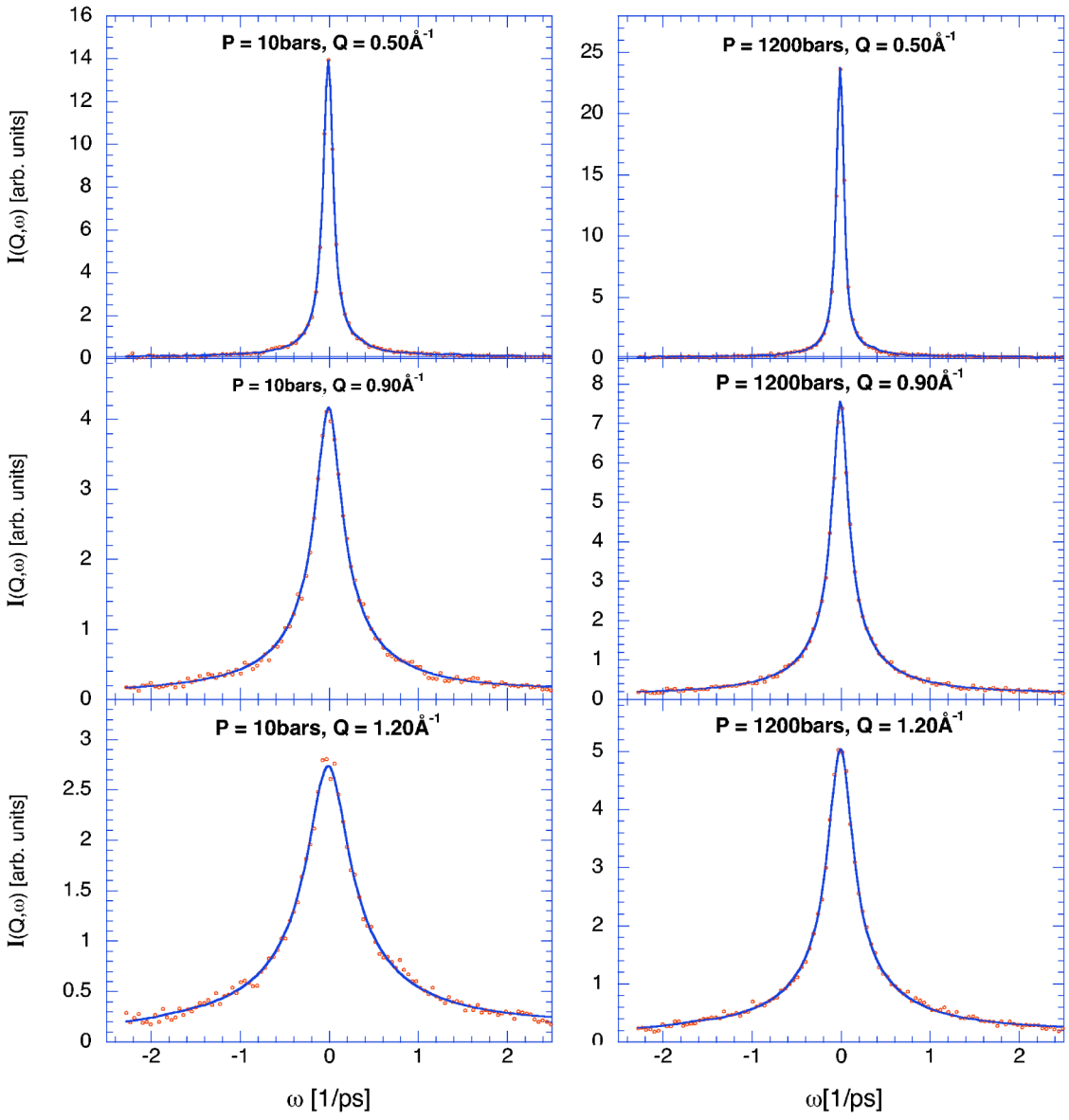

FIG. 2. Selected set of experimental (symbols) and fitted (solid lines) spectra for the momentum transfers and pressures given in the inset.

The rotational and translational diffusion coefficients derived from the fits are shown in Fig. 3. A glance at the referred figure shows that the pressure dependence of both diffusion coefficients displays a nontrivial behavior. There is a monotonous decrease in both diffusion coefficients with increasing pressures up to 200 bars and a subsequent change of regime at a point where both translation and rotation change their pressure dependence. The translational diffusion coefficients thus attain a plateau value at about 400 bars and then a further decrease. The slope for D_{trans} decreases in absolute value from a low pressure value of -1.50×10^{-4} to -0.62×10^{-4} Å^2 ps^{-1} bar^{-1} past the inflection range. On the other hand, the rotational coefficient seems to increase its value from 0.068 ± 0.037 to 0.077 ± 0.046 ps^{-1} just after the point of inflection. At higher pressures it continues decreasing with a smaller slope (-5.4×10^{-5} below and -1.3×10^{-5} ps^{-1} bar^{-1} for pressures above those signaling the anomaly).

The presence of such an inflection point is indicative of some local molecular rearrangement induced by the increase in density. Whether this corresponds to structural or purely dynamic phenomena is discussed later on. A point which is worth remarking on here is that such an anomaly takes place at pressures close to those where the miscibility loop of 2MP/D_2O shrinks towards a double critical point.

Comparison of the results here obtained with those published for 3MP [7] under similar conditions (T_{2MP}=40 °C, P_{2MP}=10 bars; T_{3MP}=38 °C, P_{3MP}=1 bar) it is found that although the densities of 2MP and 3MP are similar (0.944 and 0.956 g/cm^3), the molecular movements of the 2MP are faster than that of 3MP ($D_r^{2MP}\sim1.9D_{\rm rot}^{3MP}$ and $D_T^{2MP}\sim1.7D_T^{3MP}$). The immiscibility loop is much smaller in the 2MP/D_2O reentrant solutions than in the 3MP/D_2O case (approximately 30 °C and 80 °C, respectively) the differences being in the lower critical point (~38 °C for 3MP and ~86 °C for 2MP) [3,8].

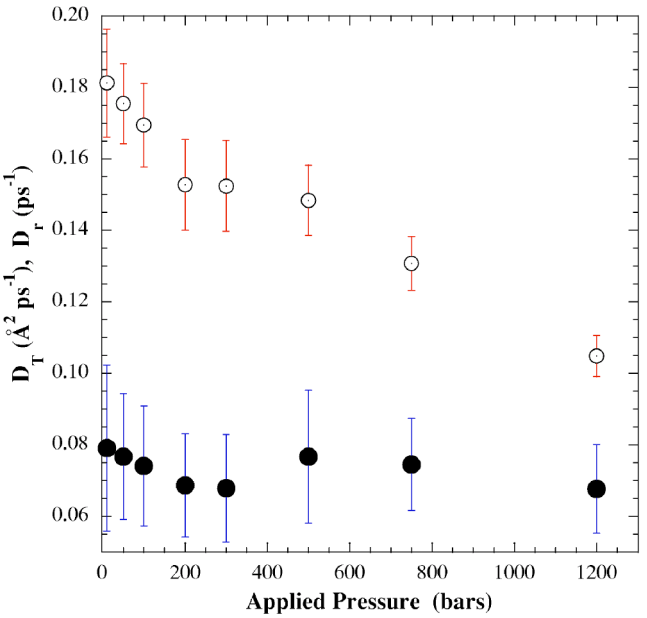

FIG. 3. Pressure dependence of the translational (open circles with a dot) and rotational (solid circles) coefficients as derived from analysis of experimental spectra.

IV. COMPUTER SIMULATIONS

A set of molecular dynamics simulations spanning 17 different densities has been carried out in order to access quantities not easily amenable to experiment. This is done in order to improve some aspects of the analysis of experimental spectra particularly those concerning molecular reorientations where the assumption of isotropic rotational diffusion may be too strong to hold for a liquid composed of oblate-shaped particles.

The molecular model here employed uses six interaction sites per molecule corresponding to N, CH, and CH_3 moieties. The interaction potential comprises Lennard-Jones and electrostatic interactions with parameters taken from Jorgensen's OPLS force field [12]. The parameter set has previously been used to study some properties of liquid pyridine [13], and a list of their corresponding values is given in Table I.

The simulations were performed using the DL_POLY package [14] on systems consisting of 216 molecules enclosed in a cubic box with periodic boundary conditions and a time step of 2 fs. The van der Waals interactions were truncated using a cutoff radius of 12.5 Å and the long-range electrostatic interactions were taken into account using the Ewald method [15]. Three different sets of simulations were carried out. A first group of calculations was performed on the microcanonical ensemble (constant *NVE*) at an average temperature close to 298 K and 17 densities comprising the 0.924–0.994 g cm^{-3} range. Simulations using a Nose-Hoover thermostat were carried out for 12 different densities. Also, an additional group of 14 simulations was carried out using the Berendsen thermostat. The latter two groups of simulations were carried out in order to study in detail the effects of temperature and pressure fluctuations on the obtained transport coefficients. When using the Berendsen algorithm, a study of the dependence of the relaxation time was also conducted. All in all, the effects of temperature and pressure fluctuations were found to be small but systematic and therefore the calculated quantities are given as averages taken over the whole sets of simulations.

TABLE I. Lennard-Jones potential parameters (ϵ, σ) and fractional electric charges on atoms. Carbons C-1 (α) are located at both sides of nitrogen. The C-3 (γ) carbon lies opposite to nitrogen and the two C-2 (β) carbons are located at both sides of C-3.

Center	ε (kJ/mol)	σ (Å)	Electric charge (e)
N	0.71	3.25	−0.49
CH_3	0.67	3.91	0.0
C-1 (α)	0.46	3.75	0.23
C-2 (β))	0.46	3.75	−0.03
C-3 (γ)	0.46	3.75	0.09

The first simulation was done at a density slightly lower than experiment and the system was subsequently compressed in a progressive way in order to determine the effect of the pressure on the system dynamics. In total we have done 42 different simulations. Each simulation consisted of the compression phase, followed by an equilibration period of 10^5 steps (i.e., 200 ps), and a production phase of 2×10^5 steps (400 ps) where the trajectories were saved every 0.05 ps in order to study the system dynamics.

A. Microscopic structure

The calculated $g(r)$ radial distribution functions for the simulated liquid are shown in Fig. 4. The quantities there displayed correspond to a sum involving the seven pseudoatoms comprising the molecular model used in the simulations (see Table I) and are labeled as $g_{at}(r)$ to distinguish them from the $g_{c.m.}(r)$ radial distributions calculated for the set of molecular centers of mass which are displayed in Fig. 5.

The data shown in Fig. 5 serve to attest to the scant difference in the distribution of molecular centers with increasing density. In fact, the most noticeable differences concern the heights of the first shoulder located at about 4.15 Å as well as that of the main peak at 6.0 Å, while their characteristic distances remain unaffected by a change in density of ≈7%.

In contrast to the radial distributions pertaining the molecular centers of mass, the atom-atom quantities shown in Fig. 4 display a systematic variation with increasing density. In short, the two most prominent peaks located at ≈4.5 Å and 6.0 Å witness an intensity increase for the former and a concomitant decrease for the latter as density increases. This is also accompanied by a shift in the position of the first peak towards closer distances. An aspect worth dwelling on concerns the presence of two *isosbestic points* located at about 5 Å and 7.4 Å where all curves cross each other. The significance of such points has been discussed previously within the context of liquid water [16]. There, in common with most results concerning optical absorption spectra, the presence of

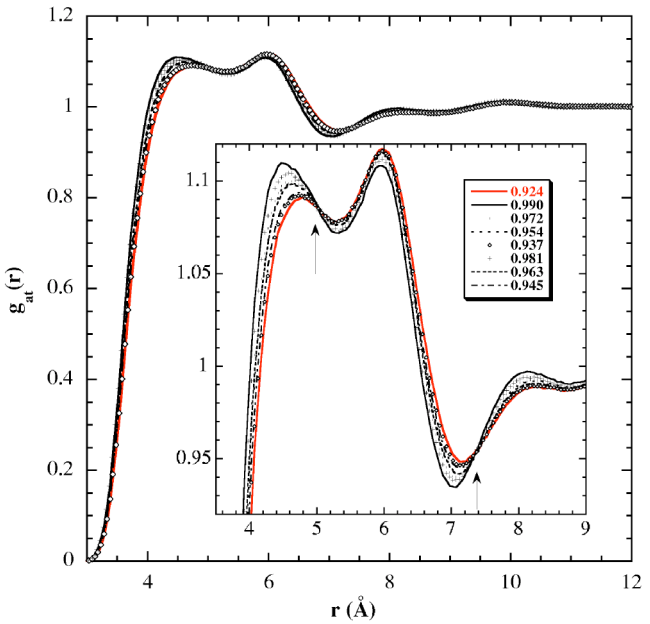

FIG. 4. Calculated radial distribution functions for the eight different densities. The values expressed in g cm^{-3} are given within the inset. The latter shows a blowup of the region comprising the two points at ≈5 Å and 7.35 Å where all curves intersect (isosbestic points) and are signaled by vertical arrows.

such singularities is interpreted as the signature of an underlying equilibrium between two (or more) different species.

To quantify the extent of molecular orientational correlations together with their density dependences, the static orientational correlation functions $G_l(r)=\langle \boldsymbol{\mu}^i \cdot \boldsymbol{\mu}^j \rangle$ have been evaluated. Such quantities specify the average value of the correlator for the relative orientation of the molecular dipole

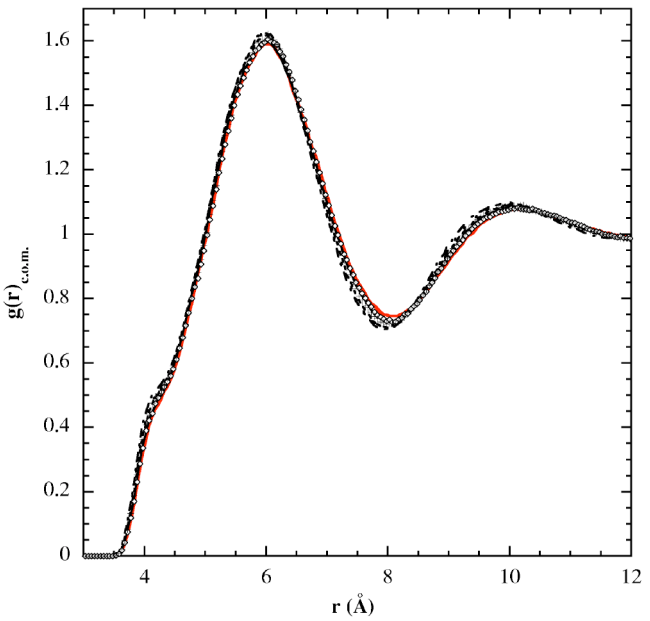

FIG. 5. Calculated radial distribution fuctions corresponding to the molecular centers of mass for the eight different densities. Symbols are the same as those used in Fig. 4.

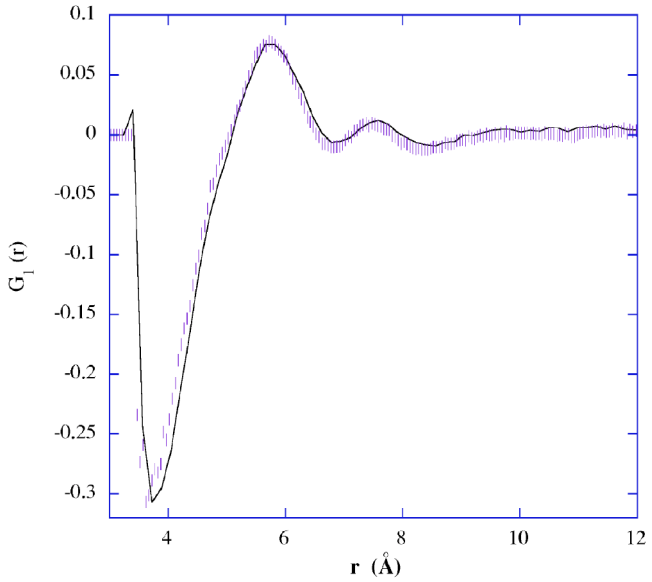

FIG. 6. Calculated first-rank orientational correlation functions corresponding to vectors taken along the molecular dipole moments for the lowest (solid line) and highest (vertical bars) densities.

moments with increasing distance between their molecular c.m. The lowest order correlation function of such a kind $G_l(r)=\langle \boldsymbol{\mu}^i \cdot \boldsymbol{\mu}^j \rangle$ just gives the average value of the vector product of dipole moment vectors sitting in different molecules. The result is shown in Fig. 6 for data comprising the two extreme densities.

The data displayed in Fig. 6 show that strong orientational correlations persist up to ≈9 Å. This corresponds to distances comprising up to next-nearest neighbors, an account made of the graphs shown in Fig. 5. The interesting point to remark is the strong antiferroelectric ordering present at contact distances (3.5–5 Å) which correspond to those about the lowest distance shoulder in $g_{c.m.}(r)$. This is followed by two oscillations centered about 5.7 Å and 7.5 Å depicting a parallel (ferroelectric) alignment of molecular dipoles that takes place at distances where $g_{c.m.}(r)$ shows its main peak. Finally, any clear hint of correlation in molecular orientation is lost for distances comprising the third coordination shell, i.e., about 10 Å where $g_{c.m.}(r)$ shows the last oscillation. As regards the density dependence of such functions, data shown in Fig. 6 attest to the fact that its main effect is to phase-shift the oscillations towards lower distances.

B. Stochastic dynamics

An isotropic average of the translational diffusion coefficient was derived from a linear fit of the long-time dependence of the mean-square displacements using the known Einstein formula

$$D_T = \lim_{t\to\infty} \frac{\langle |r(t)-r(0)|^2 \rangle}{6t}. \tag{2}$$

The results are depicted in Fig. 7 where a clear change of regime is seen for densities 0.96–0.98 g cm^{-3}.

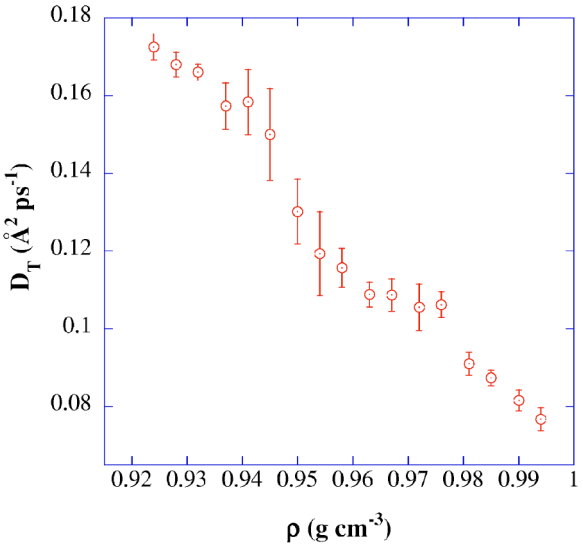

FIG. 7. Density dependence of the translational self-diffusion coefficients as estimated from Eq. (2). The error bars represent systematic errors calculated from averages taken over the whole set of simulations.

Additional details of the microscopic molecular motions are provided by the time-dependent orientational correlation function (OCF)

$$C_l(t) = \langle \mathbf{u}_l^{\alpha}(t) \cdot \mathbf{u}_l^{\alpha}(0) \rangle = P_l(\cos\,\theta_{\alpha}), \tag{3}$$

where $u^{1,2,3}$ stands for a unit vector following some specified direction in the molecular frame, P_l is a Legendre polynomial of lth order, and $\theta_{1,2,3}$ are angles subtended between the unit vectors just referred to and the axis of a laboratory frame. The molecule-fixed axes were chosen making one of them (axis 2) to coincide with the direction of the molecular dipole moment, a second normal to it also within the molecular plane (axis 1) and a third perpendicular to both (axis 3).

An example of the orientational correlations just referred to is shown in Fig. 8 for the three vectors just referred to and two densities. The first-order orientational correlations $C_1^{1,2,3}(t)$ shown in Fig. 8 display an initial Gaussian decay for times less than 1 ps followed by purely exponential relaxations that extend to long times ($\approx$50 ps). Each relaxation is characterized by a decay constant $D_{1,2,3}$ which is directly related to the diagonal elements of the rotational diffusion tensor for an asymmetric-oblate ellipsoid.

The density dependence of average rotational constants is shown in the upper frame of Fig. 8. There one sees how a change of regime with increasing density takes place for densities about ρ=0.965 g/cm$_3$. Such average rotational diffusion constants are defined as

$$D_S = \frac{1}{3}(D_1 + D_2 + D_3),\; D_{\text{plate}} = \frac{12D_1(D_1 + 2D_3)}{6(5D_1 + D_3)} \tag{4}$$

and correspond to an isotropic average over the three diffusion constants as well as to the case where the molecule is viewed as a circular plate [17]. A comparison of both coefficients serves to quantify the extent of motional anisotropy, which is seen to be small but systematic. In other words, the molecular reorientation for the range of explored densities shows a measurable anisotropy which is to be considered as a relatively minor deviation from the isotropic reorientation regime, an account made of the achievable statistics. On such

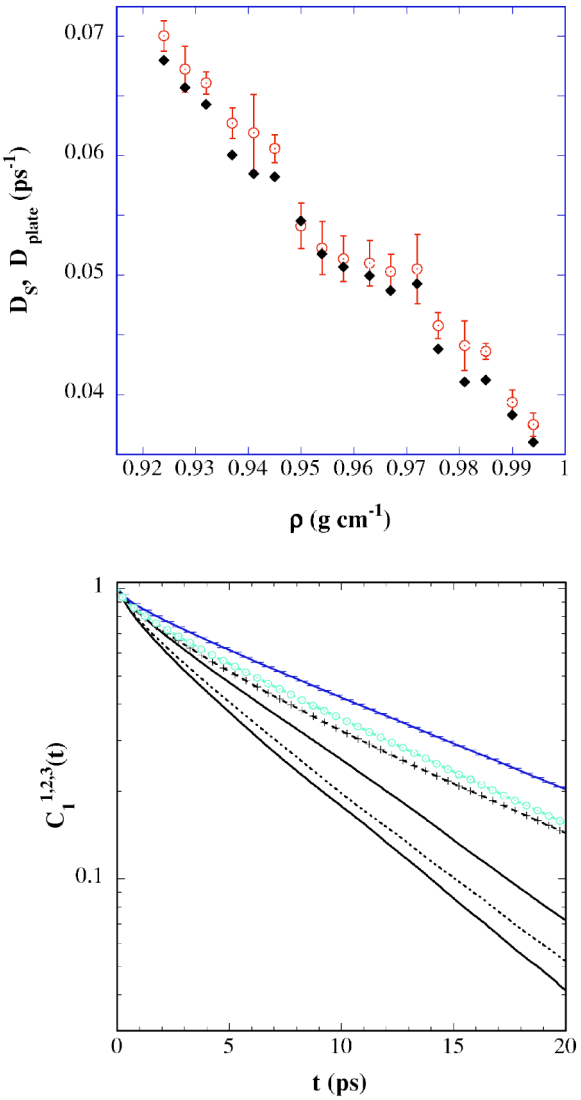

FIG. 8. The upper frame displays the density dependence of the $D_{S,\text{plate}}$ reorientational diffusion coefficients corresponding to the isotropic average of the three diffusion constants D_i (circles with a dot) and the D_{plate} average value as calculated for a circular plate (solid lozenges). Error bars shown for D_S correspond to systematic errors calculated over the whole set of simulations. Error bars for D_{plate} are omitted for the sake of clarity. The lower frame displays the $C_1^{1,2,3}(t)$ orientational relaxation functions corresponding to two in-plane (1,2) and out-of-plane axes (3) for the lowest ρ=0.924 g cm^{-3} and highest ρ=0.994 g cm^{-3} densities. Lines depict reorientation about axis 1 (solid), 2 (long dashes), and 3 (dots) for the lowest density. Lines with symbols show relaxations for the higher density. Lines with horizontal bars depict relaxation for axis 1, crosses show axis 2, and circles correspond to axis 3.

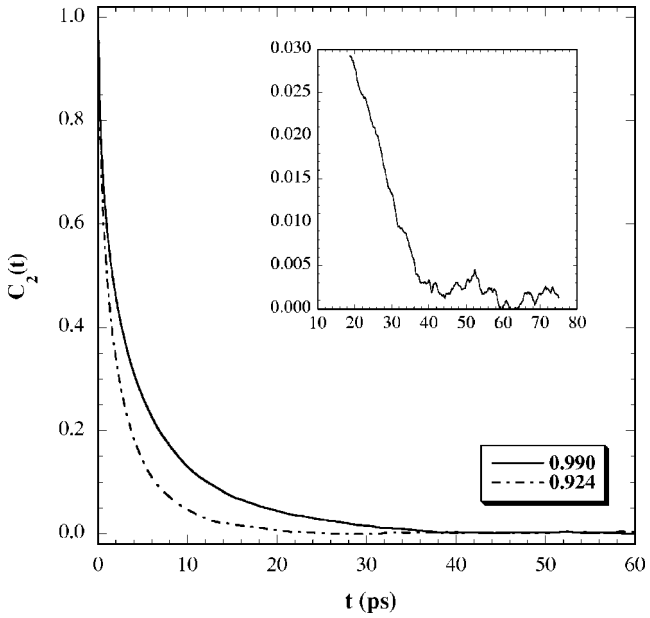

FIG. 9. Second-order orientational correlation functions for the axis normal to the molecular plane at the two extreme densities. The inset depicts the long-time contribution estimated by subtraction from the calculated $C_2(t)$ of a model function consisting on an initial Gaussian plus an exponential relaxation (see text).

grounds we will take the isotropic diffusion coefficient D_S as the relevant quantity to compare with the experimental D_R.

The curves shown in Fig. 9 depict an example of the second-order OCF. The observed trends follow those just discussed for the first-order relaxation. Quantitative analysis of such relaxations gets somewhat more complicated since these functions show a small additional component at long times or a long-time tail which may be approximated by an algebraic power law such as $a\ t^{-\zeta}$. The origin of the latter contribution seems to be specific to reorientations of oblate particles as described in detail in Ref. [18]. Fully quantitative estimates of the ζ exponents were, however, hampered by the rather high statistics required to isolate such a weak signal from the main relaxation.

C. Calculated spectra

As explicited above, the use of a crude diffusion approximation to model the experimental intensity and subsequently extract dynamic information is validated by simulation results that show that both the mass and rotational dynamics can be safely treated on such grounds. Even more, the effect on the non-negligible anisotropy in the molecular reorientations has been quantified and found to result in a systematic underestimation of the average isotropic rotational diffusion coefficient by 7%.

Also, the $F_s(Q,t)$ self-intermediate scattering function was obtained from the simulations for different mass densities of the liquid. The long-time part of the center-of-mass intermediate functions, $F_s(Q,t)_{\text{c.m.}}$, were fitted to an exponential decay as it is predicted by the Fick translational diffusion model. The exponent factors multiplying the time (the translational width in ω space) were obtained as parameters of the fit, and after, they were included as fixed data in the analysis of the atomic intermediate scattering functions $F_s(Q,t)$, thus restricting the number of the adjustable parameters. The model used for the purpose was the same described above for the experimental data analysis, and the rotational diffusion coefficient was obtained as a parameter.

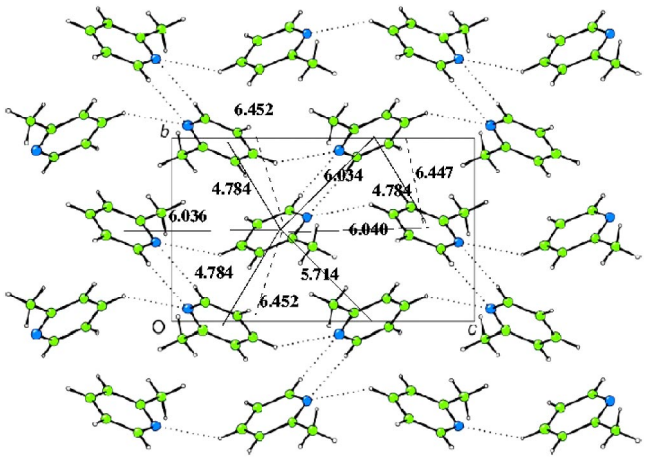

FIG. 10. A projection onto (100) showing the molecular packing in 2MP as described in [19].

Scrutiny of the accuracy of the simulation results versus experiment can be carried out. For pressures of 1 bar, corresponding to a density of $\rho=0.944\ \text{g/cm}^3$, the translational and rotational diffusion coefficients yield ($D_T^{\text{expt}} \simeq 0.181\text{Å}^2\ \text{ps}^{-1}$, $D_T^{\text{sim}} \simeq 0.133\text{Å}^2\ \text{ps}^{-1}$ and $D_R^{\text{expt}} \simeq 0.079\ \text{ps}^{-1}$, $D_S^{\text{sim}} \simeq 0.061\text{ps}^{-1}$ respectively). Although the simulations show quantitative differences with experiment, the density dependence of both D_T and D_S also reveals an anomaly within the range $0.955-0.975\ \text{g/cm}^3$ where both translational and rotational dynamics show a change of regime.

V. DISCUSSION

Here we will discuss the relevance of the obtained results mostly within the context of phenomena pertaining the existence of liquid →liquid transitions as presently postulated to explain a whole variety of mostly dynamic phenomena.

A. Liquid structure

The crystal structure of 2MP has been reported twice in the recent literature [19]. Both studies report an orthorhombic $P2_12_12_1$ unit cell comprising four molecules. Molecular packing shows a herringbone arrangement with clear indications of directional bonding with neighboring molecules either by C-H$\cdots$N or C-H$\cdots\pi$ electron cloud interactions. That is, the crystal data show direct evidence of the self-associating nature of this system. Pictorially, the molecular packing along (100) is shown in Fig. 10.

From such packing arrangement relevant $g_{at}(r)$ and $g_{c.m.}(r)$ have been calculated and are compared to the liquid structure functions in Fig. 11.

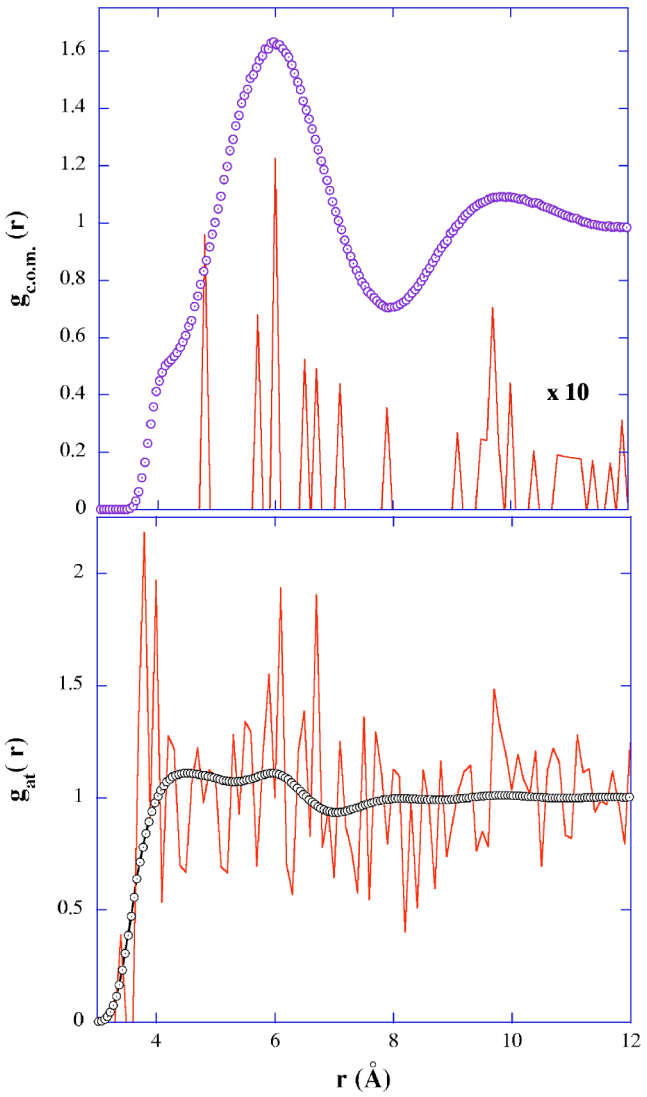

FIG. 11. The upper frame shows a comparison between the calculated $g_{c.m.}(r)$ for the liquid at a density of 0.990 g cm^{-3} (symbols) with that resulting from the crystal. Notice the scale factor that applies to the crystal data. The lower frame shows a comparison between the distributions $g_{at}(r)$ for the molecular centers of mass of crystal (line) and liquid (symbols). In order to enable a direct comparison, the calculation has been made on the same grounds as the simulation—that is, including all the hydrogens within the closest carbon as pseudoatoms.

The most striking feature of plots shown in Fig. 11 concerns the absence within the crystal structure of any feature matching the intensity of the shoulder appearing in the liquid $g_{c.m.}(r)$ at about 4.2 Å. The result is of interest since the crystal density 1.117 g cm^{-3} exceeds our maximum density by about 13% and therefore one would expect within the crystal a more closely packed structure than the liquid. The comparison of atom-atom functions also shown in the figure in contrast with the c.m. functions shows less marked differences in the contact region. The graphs compared in the lower frame of Fig. 11 show that the liquid radial distribution, apart from the low-r feature just referred to, follows in its oscillations most of the details shown by the crystal. Put into different words, the comparison just discussed points towards the presence within the liquid of local structures closer packed than within the crystal having a concentration that increases with increasing density. Data at hand as discussed by Vorontsov *et al.* [19] identify local configurations where two molecules adopt a **T** configuration that is having the molecular planes normal to each other, as able to explain such features as well as the presence of crossing (isosbestic) points in the density dependence of the atom-atom functions. In fact, such local configurations are found in the crystal structure of the positional isomer 4-methyl-pyridine [20,21] which shows at low temperatures a tetragonal $I4_1/a$ with eight molecules per unit cell having the rotational axis of the methyl groups aligned along the crystal c axis.

B. Findings in other systems

Here we consider the present results within the context of others found for liquids composed of oblatelike spheroidal particles.

The data for a number of liquids composed of planar molecules reported so far [22–24] have evidenced the presence of some change of regime at a given temperature (or pressure) that manifests itself as a change in slope of the temperature dependence of the specific heat, nuclear magnetic relaxation rate, or any other dynamical property. It has been interpreted [24,25] as a dynamical transition within the liquid state. In fact, for most systems the findings at microscopic scales can be correlated with well-defined features in macroscopic thermodynamic quantities such as the specific heat [24,26] or even some transport properties such macroscopic shear viscosity and surface tension [27] which may show a noticeable curvature within a restricted range of temperatures. In short, the temperature dependence of the specific heat and viscosity follows a behavior qualitatively similar to that shown by microscopic probes such as the NMR relaxation rates or other diffusion coefficients determined by neutron scattering, and therefore it is the presence of some nonmonotous behavior in both microscopic and macroscopic probes that gives support to the dynamic transition view. Liquid quinoline is perhaps the most widely studied system of this kind. Its basic thermophysical properties show a number of features of interest such as the isobaric thermal expansion coefficient [26] which behaves in a fairly anomalous way, showing all curves measured at a given temperature crossing point at pressures of about 500 bars. This phenomenon is rationalized on the basis of the weakly associating nature of the liquid, and indeed, the isobaric heat capacity of the liquid that shows a well-defined pressure-dependent minimum is understood on the basis of contributions from fraction of unassociated liquid plus a contribution from the enthalpy of association. The picture drawn here resembles in some respects that proposed to explain a good set of properties of liquid water in terms of a two-state model [16]. Such a conceptual framework can also explain the negative dispersion of hypersonic velocity reported in Ref. [28].

VI. CONCLUSIONS

In search for the double critical point of the mixture of 2MP and heavy water we came across a remarkable anomaly appearing within 2MP neat liquid at applied pressures of about 200 bars. It manifests itself as a marked change of regime of the translation and rotational-diffusion coefficients versus density (pressure). To add more intrigue, the pressure range at which such an anomaly takes place basically coincides with that where the DCP shown in Fig. 1 is located.

The same phenomenon has been reproduced by means of molecular simulations. This first serves to rule out any experimental artifact as an explanation for the observed anomaly. Second, the molecular simulations served to verify the procedure employed for the analysis of experimental spectra as well as to gain access to quantities not easily amenable to experiment. In particular, computer experiments have validated the use of the model given by Eq. (1) since the motional anisotropy was proved to be small.

The picture that emerges from the present study portrays the interactions within these liquid materials as substantially more complex than initially though of [3] since the liquid by itself behaves as a weakly associated entity.

[1] J.D. Cox, J. Chem. Soc. 4606 (1952).

[2] C.S. Hudson, Z. Phys. Chem., Stoechiom. Verwandtschaftsl. **47**, 113 (1904).

[3] T. Narayanan and A. Kumar, Phys. Rep. **249**, 135 (1994).

[4] J. Jacob, M.A. Anisimov, J.V. Sengers, A. Oleinikova, H. Weingartner, and A. Kumar Phys. Chem. Chem. Phys. **3**, 829 (2001).

[5] J. Jacob, A. Kumar, S. Asokan, D. Sen, R. Chitra, and S. Mazumder, Chem. Phys. Lett. **304**, 180 (1999).

[6] J. Jacob, D. Bagchi, A. Kumar, and S.L. Oswal, Physica A **318**, 101 (2003).

[7] A. Maira-Vidal, M.A. Gonzalez, C. Cabrillo, F.J. Bermejo, M. Jimenez-Ruiz, M.L. Saboungi, T. Otomo, F. Fayon, E. Enciso, and D.L. Price, Chem. Phys. **292**, 273 (2003).

[8] G.M. Schneider, Ber. Bunsenges. Phys. Chem. **76**, 325 (1972); C.W. Garland and K. Nishigaki, J. Chem. Phys. **65**, 5928 (1976).

[9] F. Rieutord (unpublished).

[10] V.F. Sears, Can. J. Phys. **44**, 1299 (1996).

[11] J.B. Lambert, R.J. Nienhuis, and R.B. Finzel, J. Phys. Chem. **85**, 1170 (1981).

[12] W.L. Jorgensen and N.A. McDonald, J. Mol. Struct.: THEOCHEM **424**, 145 (1998).

[13] I. Bako, T. Radnai, and G. Palinkas, Z. Naturforsch., A: Phys. Sci. **51**, 859 (1996).

[14] http://www.cse.clrc.ac.uk/msi/software/DLPOLY/

[15] M.P. Allen and D. Tildesley, *Computer Simulation of Liquids* (Clarendon, Oxford, 1987).

[16] G.W. Robinson, C.H. Cho, and J. Urquidi, J. Chem. Phys. **111**, 698 (1999); see also C.H. Cho, J. Urquidi, G.I. Gellene, and G.W. Robinson, *ibid.* **114**, 3157 (2001).

[17] J.M. McConell, *The Theory of Nuclear Magnetic Relaxation in Liquids* (Cambridge University Press, Cambdridge, UK, 1987), p. 85.

[18] R. Vasanthi, S. Battacharyya, and B. Bagchi, J. Chem. Phys. **116**, 1092 (2002).

[19] A.D. Bond and J.E. Davies, Acta Crystallogr., Sect. E: Struct. Rep. Online **E57**, 01087 (2001); I.I. Vorontsov, L. Almasy, and M.Yu. Antipin, J. Mol. Struct. **610**, 217 (2002).

[20] U. Ohms, H. Guth, W. Treutmann, H. Dannöhl, A. Schweig, and Heger, J. Chem. Phys. **83**, 273 (1985).

[21] F. Fillaux, B. Nicolaia, W. Paulus, E. Kaiser-Morris, and A. Cousson, Phys. Rev. B **68**, 224301 (2003).

[22] F.J. Bermejo, M. Garcia-Hernandez, W.S. Howells, R. Burriel, F.J. Mompen, and D. Martin, Phys. Rev. E **48**, 2766 (1993).

[23] L. Letamendia, M. Belkadi, O. Eloutassi, E. Pru-Lestret, G. Nouchi, J. Rouch, D. Blaudez, F. Mallamace, N. Micali, and C. Vasi, Phys. Rev. E **54**, 5327 (1996); C.H. Chung and S. Yip, Phys. Rev. A **4**, 928 (1971).

[24] J.B. Robert, J.C. Boubel, and D. Canet, Mol. Phys. **90**, 399 (1997).

[25] N.B. Rozhdesvenskaya and L.V. Smirnova, J. Chem. Phys. **95**, 1223 (1991).

[26] S.L. Randzio, D.J. Eautough, E.A. Lewis, and L.D. Hansen, Int. J. Thermophys. **17**, 405 (1996).

[27] L.R. Grzyll, C. Ramos, and D.D. Back, J. Chem. Eng. Data **41**, 446 (1996).

[28] L.M. Kashaeva, L.M Savirov, Sh. Sidikov, T.M. Utarova, and Ya.T. Turakov, Acoust. Phys. **44**, 312 (1998).